Japanese Journal of Applied Physics

SELECTED TOPICS IN APPLIED PHYSICS

Effect of interface NiO layer on magnetism in Fe/$BaTiO_3$ thin film

Japanese Journal of Applied Physics **57**, 0902B9 (2018)
https://doi.org/10.7567/JJAP.57.0902B9

Effect of interface NiO layer on magnetism in Fe/$BaTiO_3$ thin film

Masako Sakamaki[1,2*] and Kenta Amemiya[1,2]

[1]*Institute of Materials Structure Science, High Energy Accelerator Research Organization, Tsukuba, Ibaraki 805-0801, Japan*
[2]*Department of Materials Structure Science, School of High Energy Accelerator Science, The Graduate University for Advanced Studies (SOKENDAI), Tsukuba, Ibaraki 305-0801, Japan*

*E-mail: masako.sakamaki@kek.jp

Received January 31, 2018; accepted April 7, 2018; published online June 27, 2018

The insertion effect of an interface NiO layer on magnetism in Fe/$BaTiO_3$ is investigated by X-ray absorption spectroscopy (XAS). From X-ray magnetic circular dichroism (XMCD) analysis, the enhancement of remanent magnetization in Fe is observed with increasing NiO thickness. We also find that the NiO layer is partially composed of metallic Ni, and its thickness is estimated to be ~0.4 nm from the NiO-thickness dependence of the Ni XAS intensity by assuming that Ni is localized at the interface between Fe and NiO. Moreover, extended X-ray absorption fine structure data shows that the Ni–O distance of the interface NiO layer is shorter than that of bulk NiO, which leads to the pseudomorphic growth of NiO on $BaTiO_3$. We thus suppose that the improved Fe growth promoted by the interface NiO layer enhances the magnetic moment in Fe.

1. Introduction

Electric-field-induced magnetic switching has been intensively studied so far because of its great potential to reduce the energy consumption of the switching process in nanometer-scale magnets.[1–6] The ferromagnetic–ferroelectric heterostructure is a simple case of controlling magnetism by applying an electric field to ferroelectric materials. In that sense, we focus on a simple multiferroic heterostructure, Fe/$BaTiO_3$, and observe its interface state with the aim of controlling the magnetoelectric effect. Magnetic and electric manipulations of $BaTiO_3$-based multiferroic heterostructures have been extensively studied recently.[7–11] It was reported that the coercive field of an Fe thin film grown on $BaTiO_3$ changes when an electric field is applied between the Fe film and the bottom of $BaTiO_3$.[12,13] Some theoretical calculations suggest that such field-induced change is due to the hybridization between Ti 3d–O 2p and Fe 3d at the interface.[14,15] However, direct observation of the interface state has not been reported. We have recently found from X-ray absorption spectroscopy (XAS) and X-ray magnetic circular dichroism (XMCD) that an Fe oxide component exists near the interface, and that it closely correlates with the field-induced magnetic change in Fe.[16] In this study, we insert an interface NiO layer between the Fe thin film and $BaTiO_3$ for realizing peculiar interface phenomena, such as the ferromagnetic/antiferromagnetic coupling between Fe and NiO. Although our final goal is to utilize such interfacial effect and apply it to the field effect, here, we concentrate on the investigation of the effect of the interface NiO layer on the magnetism of Fe/$BaTiO_3$ by using XMCD and extended X-ray absorption spectroscopy (EXAFS), and a possible interfacial structure is discussed.

2. Experimental procedure

XMCD experiments were performed at the soft X-ray undulator beamline BL-16A of Photon Factory, Japan.[17] The polarization switching between opposite circular polarizations was also applied[18,19] to XMCD hysteresis measurement. NiO films were grown on a 0.5-mm-thick $BaTiO_3$(001) substrate in a high-vacuum chamber at room temperature by O_2-reactive evaporation from a Ni rod by electron bombardment. Wedge-shaped NiO films were prepared, in which the thickness was altered from 0 to 3 nm, then a 2-nm-thick Fe film was grown on that. The film was then covered with Au by the electron bombardment evaporation of Au in a Mo crucible at room temperature in order to protect the films from oxidation.

The XMCD spectra were taken at room temperature under the grazing incidence condition, in which the angle between the surface normal and the X-ray beam was 60°, because the films show in-plane magnetization. The magnetic fields of ±250 Oe were applied along the incident X-ray beam during the XMCD measurement. The XMCD-hysteresis curves were obtained by measuring the XMCD intensity at the L_3 peak top (708.5 eV) as a function of magnetic field. The XMCD intensity is defined as a difference in absorption intensities between right and left circular polarizations divided by an averaged peak intensity.

The Ni and Fe K-edge EXAFS spectra were measured at the bending magnet beamline, BL-12C, of Photon Factory, Japan. All the spectra were recorded at room temperature in the fluorescence-yield mode with a 19-element solid-state detector. To examine the crystallographic structure of Ni and Fe sites, the EXAFS spectra were taken at normal incidence configuration, in which structural information in the in-plane direction is sensitively obtained.

3. Results and discussion

Figure 1 shows Fe L-edge XAS, μ^+ and μ^-, and XMCD, $\mu^+-\mu^-$, spectra of Fe (2 nm)/$BaTiO_3$ and Fe (2 nm)/NiO (2.25 nm)/$BaTiO_3$ thin films. The spectral shapes of XAS and XMCD of the films do not show a big change, but the XMCD intensity is larger in the case of the Fe (2 nm)/NiO (2.25 nm)/$BaTiO_3$.

Then, we look at the XMCD-hysteresis curves of the Fe (2 nm)/NiO (0–3 nm)/$BaTiO_3$ thin film measured at the Fe L_3 absorption edge at 708.5 eV with different NiO thicknesses, t_{NiO}, as shown in Fig. 2. All the curves show relatively good squareness, which indicates that the Fe film shows almost the same in-plane magnetic anisotropy at any NiO thickness. On the other hand, the remanent magnetization increases as the thickness increases, as is also the case with the XMCD spectra in Fig. 1. To determine the factor that makes the remanent magnetization smaller for the films with thinner or without NiO, we look at the chemical state and structure of Ni in detail.

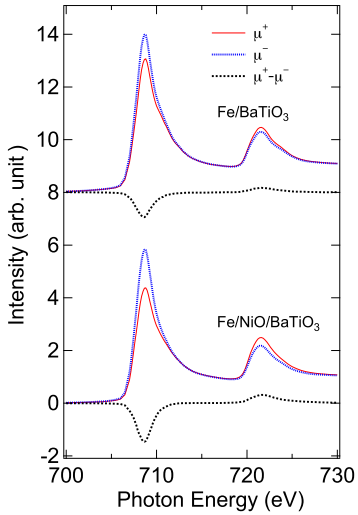

Fig. 1. (Color online) Fe L-edge XAS, μ^+ and μ^-, and XMCD, $\mu^+-\mu^-$, spectra of Fe (2 nm)/$BaTiO_3$ and Fe (2 nm)/NiO (2.25 nm)/$BaTiO_3$ thin films.

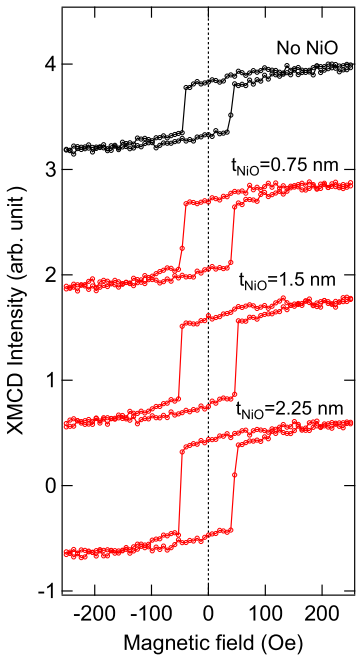

Fig. 2. (Color online) XMCD-hysteresis curves of Fe (2 nm)/NiO (0–3 nm)/$BaTiO_3$ thin film with different t_{NiO} values measured at Fe L_3 absorption edge (708.5 eV).

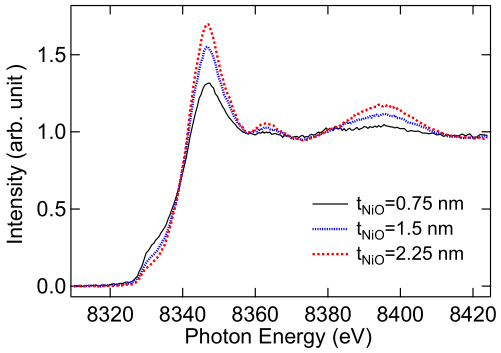

Fig. 3. (Color online) Ni K-edge XAS spectra of Fe (2 nm)/NiO (0–3 nm)/$BaTiO_3$ thin film with different t_{NiO} values.

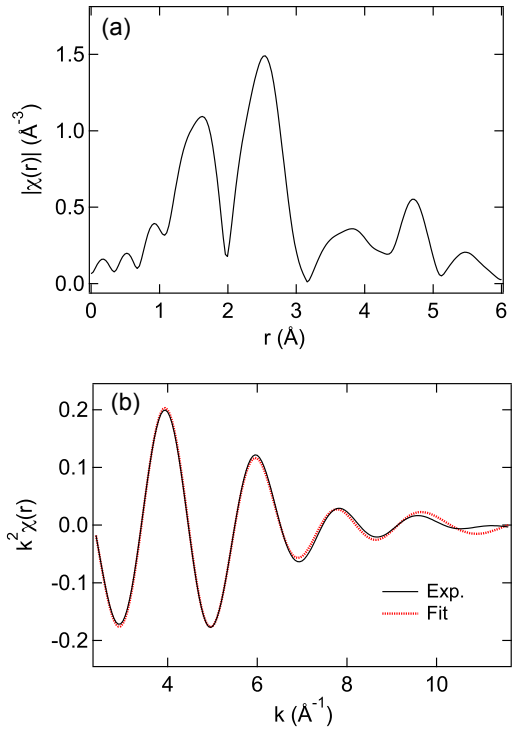

Fig. 4. (Color online) (a) Fourier transform of the Ni K-edge EXAFS function, $k^2\chi(k)$, and (b) inverse Fourier-transformed EXAFS function at the first shell of Fe (2 nm)/NiO (2.25 nm)/$BaTiO_3$ thin film. Fitted spectrum is also shown in the figure.

Figure 3 shows Ni K-edge XAS spectra of the Fe (2 nm)/NiO (0–3 nm)/$BaTiO_3$ thin film with different t_{NiO} values. The shoulder and peak structures at ~8330 and ~8345 eV are attributed to metallic Ni and NiO, respectively, according to the reference spectra.[20] This indicates that the interface NiO layer is partially composed of metallic Ni, and its component is larger for a thinner NiO, as is also observed in Ni L-edge XAS, which is not shown here. By comparing with the white line intensity of these spectra, we estimated the ratio of the metallic Ni component to the NiO component, and the thickness of the metallic Ni is determined to be ~0.4 nm if we assume that Ni is localized at the interface between Fe and NiO. Because EXAFS can detect only averaged structural information in depth, we further need depth-resolved XAS analysis[21–23] in order to determine the depth distribution of Ni.

Next, the local structure of the interface NiO layer is investigated by EXAFS measurement. Figure 4(a) shows the Fourier transform of the Ni K-edge EXAFS function of Fe (2 nm)/NiO (2.25 nm)/$BaTiO_3$ thin film. The main peaks at ~1.5 and ~2.5 Å correspond to the first nearest Ni–O and Ni–Ni bonds in the NiO rock-salt framework. In addition, there are small structures at higher coordination, ~3–5 Å, and they are considered as a mixture of Ni–O and Ni–Ni bonds. Then, we further analyze the EXAFS data of the nearest Ni–O bond because it contains solely the NiO component and no complicated analyses are required. EXAFS curve fitting is performed using the IFEFFIT package[24,25] in k (wave number) space after the inverse Fourier transformation for the nearest Ni–O contribution (1.0–3.0 Å). The EXAFS spectra for the fcc NiO[26] calculated using the FEFF8[27] code are used as a theoretical standard. Experimental and fitted

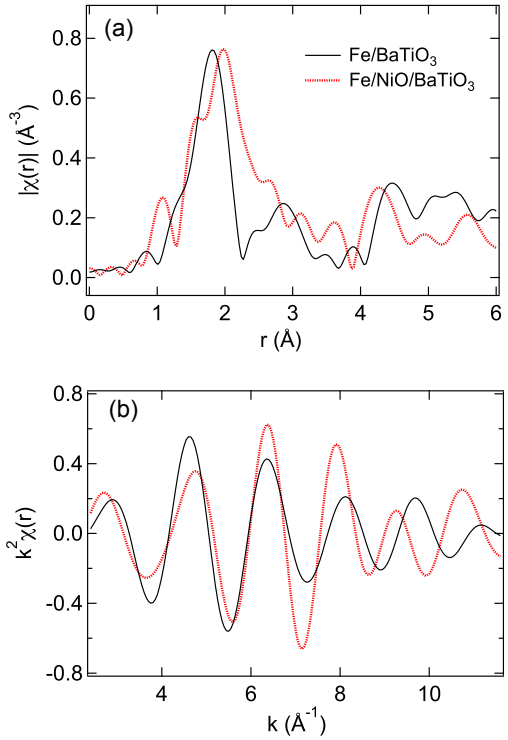

Fig. 5. (Color online) (a) Fourier transforms of the Fe K-edge EXAFS function, $k^2\chi(k)$, and (b) inverse Fourier-transformed EXAFS function at the first shell of Fe (2 nm)/$BaTiO_3$ and Fe (2 nm)/NiO (2.25 nm)/$BaTiO_3$ thin films.

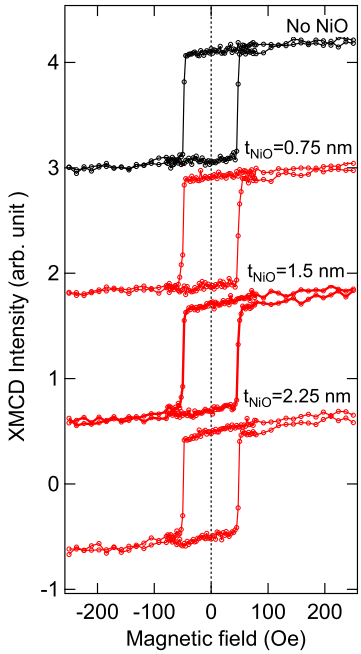

Fig. 6. (Color online) XMCD-hysteresis curves of Fe (2 nm)/NiO (0–3 nm)/$BaTiO_3$ thin film with different t_{NiO} values measured at Fe L_3 absorption edge (708.5 eV) after the heating treatment at 370 K for 10 min.

inverse Fourier-transformed EXAFS functions are displayed in Fig. 4(b). We obtained the Ni–O bond length as 2.03 Å, and estimated the in-plane lattice constant of Ni–O as 0.406 nm. By taking into account that the lattice constant of $BaTiO_3$ ($a = 0.398$ nm)[28] is smaller than that of bulk NiO ($a = 0.418$ nm),[26] it is reasonably understood that the in-plane lattice constant of NiO shrinks to coordinate with that of $BaTiO_3$, and the pseudomorphic growth of NiO is thus carried out.

Next, we look at the local structure of the Fe site. Figure 5(a) shows Fourier transforms of the Fe K-edge EXAFS function, $k^2\chi(k)$, of Fe (2 nm)/$BaTiO_3$ and Fe (2 nm)/NiO (2.25 nm)/$BaTiO_3$ thin films. The inverse Fourier-transformed EXAFS function of the first shell (1.0–2.6 Å) is also shown in Fig. 5(b). The amplitude in Fe/$BaTiO_3$ is maximum at the lower wave vector, $k \simeq 4.5$ Å^{-1}, and it rapidly decays, while in the case of Fe/NiO/$BaTiO_3$, the maximum amplitude is observed at higher k. Considering the k-dependence of the backscattering amplitude of scattering atoms, the maximum amplitude appears at lower k for lighter elements.[29,30] This is a direct confirmation that the peaks in Fig. 5(a) at ~1.8 Å in Fe/$BaTiO_3$ and ~2 Å in Fe/NiO/$BaTiO_3$ are attributed to the Fe–O and Fe–Fe bonds, respectively. Therefore, in the case of Fe/$BaTiO_3$, we suppose that the Fe layer is partially oxidized and shows a disordered structure caused by the multidomain structure of $BaTiO_3$. Consequently, the bcc-Fe framework, that is, the Fe–Fe bond is not clearly observed. These results can also be understood from the Ni EXAFS data that Fe stably grows on the NiO buffer layer possibly due to the elimination of the multidomain structure in $BaTiO_3$. We therefore assume that the NiO buffer layer suppresses the structural disorder in the Fe thin film.

To confirm the role of the NiO buffer layer, we examine the heat treatment effect on the magnetic property of the film. Figure 6 shows the XMCD-hysteresis curves measured at the Fe L_3 absorption edge at 708.5 eV of the Fe (2 nm)/NiO (0–3 nm)/$BaTiO_3$ thin film with different NiO thicknesses, t_{NiO}, after the heating at 370 K for 10 min. Both the remanent magnetization and squareness become enhanced for all the films, and no NiO thickness dependence is observed. It is reported that such heating process stabilizes the tetragonal $BaTiO_3$ phase and improves the epitaxy of the film.[12] Therefore, we suppose that such stabilized tetragonal $BaTiO_3$ can keep the Fe magnetic moment robust even without the NiO buffer layer. In the case of the as-prepared $BaTiO_3$ substrate, multidomains in the substrate may cause structural disorders in the Fe layer if we prepare Fe directly on the substrate. On the other hand, the inserted NiO layer can eliminate the effect of the domain structure of the substrate on the structure of Fe, and promotes the improved growth of the Fe layer. We thus find that the insertion of NiO as a buffer layer can enhance the Fe magnetic moment, and the next target is to realize a significant magnetic interaction at the interface as well as structural implement.

4. Conclusions

We have investigated the insertion effect of the interface NiO layer on magnetism in the Fe/$BaTiO_3$ thin film by X-ray absorption spectroscopy. From the XMCD measurement, the enhancement of remanent magnetization in Fe was observed with increasing NiO thickness. It was also found that the NiO was partially composed of metallic Ni, and its thickness was estimated to be ~0.4 nm from the NiO-thickness dependence of the Ni XAS intensity, by assuming that Ni is localized at the interface between Fe and NiO. In addition, EXAFS data showed that the Ni–O distance of the interface NiO layer is shorter than that of bulk NiO, which leads to the pseudomorphic growth of NiO on $BaTiO_3$. We thus concluded that

the improved growth of Fe promoted by the interface NiO layer enhances the magnetic moment in Fe.

Acknowledgments

The present work was performed with the approval of the Photon Factory Program Advisory Committee (Nos. 2013S2-004, 2016S2-005, 2016G569, and 2016G618). The authors are grateful for the financial support of JSPS KAKENHI Grant Numbers 25287078 and 15K17684.

1) Y. Shiota, T. Nozaki, F. Bonell, S. Murakami, T. Shinjo, and Y. Suzuki, Nat. Mater. **11**, 39 (2012).
2) T. X. Nan, Z. Y. Zhou, J. Lou, M. Liu, X. Yang, Y. Gao, S. Rand, and N. X. Sun, Appl. Phys. Lett. **100**, 132409 (2012).
3) K. Munira, S. C. Pandey, W. Kula, and G. S. Sandhu, J. Appl. Phys. **120**, 203902 (2016).
4) G. Yu, H. Lin, Y. Li, H. Zhang, and N. Sun, IEEE Trans. Magn. **53**, 5300605 (2017).
5) M. Yi, H. Zhang, and B.-X. Xu, npj Comput. Mater. **3**, 38 (2017).
6) R.-C. Peng, J.-M. Hu, K. Momeni, J.-J. Wang, L.-Q. Chen, and C.-W. Nan, Sci. Rep. **6**, 27561 (2016).
7) Y. Shirahata, R. Shiina, D. L. González, K. J. A. Franke, E. Wada, M. Itoh, N. A. Pertsev, S. van Dijken, and T. Taniyama, NPG Asia Mater. **7**, e198 (2015).
8) S. S. Pillai, H. Kojima, M. Itoh, and T. Taniyama, Appl. Phys. Lett. **107**, 072903 (2015).
9) M. Asa, L. Baldrati, C. Rinaldi, S. Bertoli, G. Radaelli, M. Cantoni, and R. Bertacco, J. Phys.: Condens. Matter **27**, 504004 (2015).
10) G. Radaelli, D. Petti, E. Plekhanov, I. Fina, P. Torelli, B. R. Salles, M. Cantoni, C. Rinaldi, D. Gutiérrez, G. Panaccione, M. Varela, S. Picozzi, J. Fontcuberta, and R. Bertacco, Nat. Commun. **5**, 3404 (2014).
11) O. Rousseau, R. Weil, S. Rohart, and A. Mougin, Sci. Rep. **6**, 23038 (2016).
12) S. Brivio, D. Petti, R. Bertacco, and J. C. Cezar, Appl. Phys. Lett. **98**, 092505 (2011).
13) G. Venkataiah, Y. Shirahata, M. Itoh, and T. Taniyama, Appl. Phys. Lett. **99**, 102506 (2011).
14) C.-G. Duan, S. S. Jaswal, and E. Y. Tsymbal, Phys. Rev. Lett. **97**, 047201 (2006).
15) P. V. Lukashev, J. D. Burton, S. S. Jaswal, and E. Y. Tsymbal, J. Phys.: Condens. Matter **24**, 226003 (2012).
16) M. Sakamaki and K. Amemiya, e-J. Surf. Sci. Nanotechnol. **13**, 139 (2015).
17) K. Amemiya, A. Toyoshima, T. Kikuchi, T. Kosuge, K. Nigorikawa, R. Sumii, and K. Ito, AIP Conf. Proc. **1234**, 295 (2010).
18) K. Amemiya, M. Sakamaki, T. Koide, K. Ito, K. Tsuchiya, K. Harada, T. Aoto, T. Shioya, T. Obina, S. Yamamoto, and Y. Kobayashi, J. Phys.: Conf. Ser. **425**, 152015 (2013).
19) K. Tsuchiya, T. Shioya, T. Aoto, K. Harada, T. Obina, M. Sakamaki, and K. Amemiya, J. Phys.: Conf. Ser. **425**, 132017 (2013).
20) D. Pan, J. K. Jian, A. Ablat, J. Liu, Y. F. Sun, and R. Wu, J. Appl. Phys. **112**, 053911 (2012).
21) K. Amemiya and M. Sakamaki, Appl. Phys. Lett. **98**, 012501 (2011).
22) K. Amemiya, Phys. Chem. Chem. Phys. **14**, 10477 (2012).
23) M. Sakamaki and K. Amemiya, Rev. Sci. Instrum. **88**, 083901 (2017).
24) M. Newville, J. Synchrotron Radiat. **8**, 322 (2001).
25) B. Ravel and M. Newville, J. Synchrotron Radiat. **12**, 537 (2005).
26) S. Sasaki, K. Fujino, and Y. Takeuchi, Proc. Jpn. Acad., Ser. B **55**, 43 (1979).
27) A. L. Ankudinov, B. Ravel, J. J. Rehr, and S. D. Conradson, Phys. Rev. B **58**, 7565 (1998).
28) R. G. Rhodes, Acta Crystallogr. **2**, 417 (1949).
29) B. K. Teo and P. A. Lee, J. Am. Chem. Soc. **101**, 2815 (1979).
30) A. G. McKale, B. W. Veal, A. P. Paulikas, S. K. Chan, and G. S. Knapp, J. Am. Chem. Soc. **110**, 3763 (1988).